Journal of Power Sources 188 (2009) 256–260

Contents lists available at ScienceDirect

Journal of Power Sources

journal homepage: www.elsevier.com/locate/jpowsour

Short communication

A planar microfabricated electrolyzer for hydrogen and oxygen generation

L. Jiang[a], B. Myer[a], K. Tellefsen[b], S. Pau[a,*]

[a] University of Arizona, College of Optical Sciences, 1630 E. University Blvd., Tucson, AZ 85721, United States
[b] Cookson Electronics Inc., 109 Corporate Blvd., South Plainfield, NJ 07080, United States

ARTICLE INFO

Article history:
Received 31 October 2008
Received in revised form
19 November 2008
Accepted 20 November 2008
Available online 3 December 2008

Keywords:
Hydrogen
Microfabrication
Electrolysis

ABSTRACT

We present the design, fabrication and testing of a microfabricated planar reactor for the hydrogen evolution reaction (HER) using thin film Pt electrodes and polydimethylsiloxane (PDMS) fluidic chamber. The reactor is designed to separate gases by flow dynamics and reactor flow is analyzed by three-dimensional finite element analysis. The planar geometry is scalable, compact and stackable. Using KOH 28 wt% electrolyte, we have achieved a hydrogen generation density of 0.23 kg h^{-1} m^{-3} and an efficiency of 48% with a flow rate of 10 ml min^{-1} and cell voltage of 3 V.

Published by Elsevier B.V.

1. Introduction

Hydrogen is an important contender for replacing fossil fuels as a clean energy source as well as an important gas used in research and industrial chemical processing. Currently, approximately 95% of the hydrogen is produced by using fossil fuel sources [1]. Using non-renewable energy resources as the primary energy source for producing hydrogen is based on economics and the widespread availability of natural gas and fuel. For hydrogen production, fossil fuel is at present simply cheaper and more abundant than any other alternative. Nonetheless, considering the limitation and environmental impact of fossil fuel, we must develop other means of generating hydrogen, especially if hydrogen is to become a significant share of the energy market. If our goal is to reduce CO_2 emission, then it is not possible to produce hydrogen on a large scale using traditional steam reforming of natural gas [2]. Electricity, at present, is only a secondary energy source used to produce hydrogen. Improving the efficiency of solar photovoltaic (PV) cells as an electrical energy source and techniques for producing hydrogen from electricity can reduce the reliance on fossil fuels and greenhouse gas emissions. The purpose of our paper is to demonstrate a microfabricated planar reactor for hydrogen generation. Our device can provide a source of hydrogen fuel and oxygen which can potentially be integrated with and powered directly by a series of photovoltaic cells [3]. Ideally, the planar electrolyzer should satisfy the following requirements: (1) the geometry is scalable and stackable and can be fabricated by low cost techniques with minimal catalyst loading, (2) the reactor should separate the hydrogen and oxygen without intermixing, (3) the device design is durable and reliable and (4) the efficiency of converting electrical power to chemical potential energy is high.

The concept of splitting water using sunlight is quite old and was suggested by J. Verne in 1874 [4]. Solar water splitting can provide a clean and renewable source of hydrogen fuel. Extensive work on generating hydrogen has been done based on direct [5], indirect thermochemical [6], biological [7] and photoelectrochemical mechanisms [8,9]. While multiple approaches to the problem of hydrogen generation exist, each approach has unique advantages and specific limitations. For the biological photosynthetic process, the conversion efficiency is typically low, generally much less than 10% [10]. In thermal hydrogen production, heat is used to convert water into hydrogen and oxygen. The process often requires high temperature (>900 K), which leads to thermal decomposition and hydrolysis of the catalysis [6]. In photo-electrochemical conversion, a semiconductor, such as n-TiO_2, is used as a photosensitizer, for the electrolysis of water to hydrogen and oxygen [11]. In this paper, we concentrate on the direct electrochemical production of hydrogen and oxygen by water electrolysis.

Commercial electrolyzers operate primarily on two technologies. One utilizes an aqueous solution of alkaline electrolytes such as potassium hydroxide. Another utilizes a solid ion-conducting electrolyte membrane. Both technologies require precious metal catalysts such as platinum (Pt). Reduction of catalyst loading and increasing cell durability are important driving parameters in reducing cost of hydrogen generation. Decomposition of water by electrolysis consists of two chemical reactions at two electrodes,

* Corresponding author. Tel.: +1 5206263908; fax: +1 5206214358.
E-mail address: spau@optics.arizona.edu (S. Pau).

0378-7753/$ – see front matter. Published by Elsevier B.V.
doi:10.1016/j.jpowsour.2008.11.099

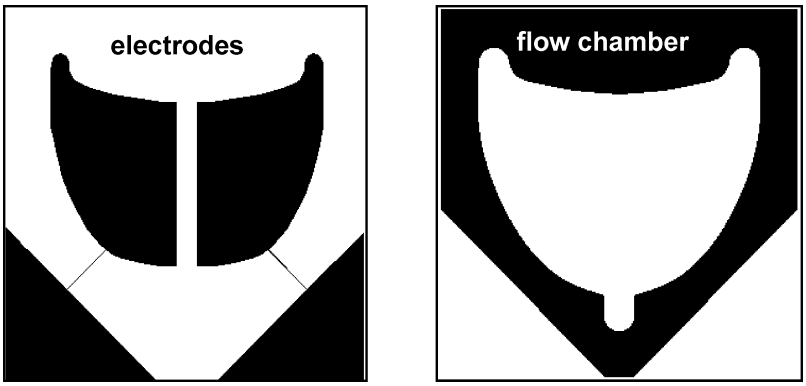

Fig. 1. Schematic diagrams of electrode and chamber layers of the planar device.

which are usually separated by a conducting electrolyte. Application of voltage across the electrodes generates hydrogen at the negative electrode (cathode) and oxygen at the positive electrode (anode). The flow of ions across the electrolyte completes the exchange of charge. A diaphragm is used to separate the cathode and anode in order to isolate the hydrogen from the oxygen. Conversion efficiency can be improved by increasing the operating pressure and temperature [12,13]. Industrial electrolyzers have electricity consumption between 4.5 and 6.0 kW h N^{-1} m^{-3} of hydrogen and an efficiency range of 65–80% [14]. Aside from conversion efficiency, an important specification for an electrolyzer is the susceptibility to fluctuations in the electrical power source [15,16]. This can be a factor if solar PV cells are the source of power under varying illumination conditions.

In this paper, we design, fabricate and test a planar electrolyzer for hydrogen generation. In Section 2, we present a three-dimensional finite element analysis of the fluid flow inside the planar electrolyzer chamber and show that our geometry can direct generated hydrogen and oxygen to separate outlets by different flow streams without intermixing. In Section 3, we present the fabrication process of the device. We have experimented with several fabrication processes and the motivations of each are discussed. In the final section, we present both electrical and flow measurements of the fabricated electrolyzer. We conclude our paper with a discussion of the device efficiency.

2. Design and simulation

Key to the planar electrolyzer is the design of the reactor geometry to efficiently separate generated hydrogen at the cathode and generated oxygen at the anode. The cathode and anode can in principle be separated far apart spatially to simplify gas removal at the expense of increased cell resistance and decreased electrolyzer efficiency. There are two degrees of freedom in the design of the planar electrolyzer: the shape of the electrodes and the shape of the reaction chamber. Schematic diagrams of both the electrodes and the chamber of the planar device are shown in Fig. 1. For a fixed device size, the surface area of the electrodes should be maximized to have large current density. A large current density will lead to high hydrogen generation for a fixed applied voltage. The configuration of the reaction chamber should be designed to provide steady flow of electrolyte and to allow separation of the gases. Our design is different from previous work which does not contain a fluidic chamber [17]. One advantage of our design is the

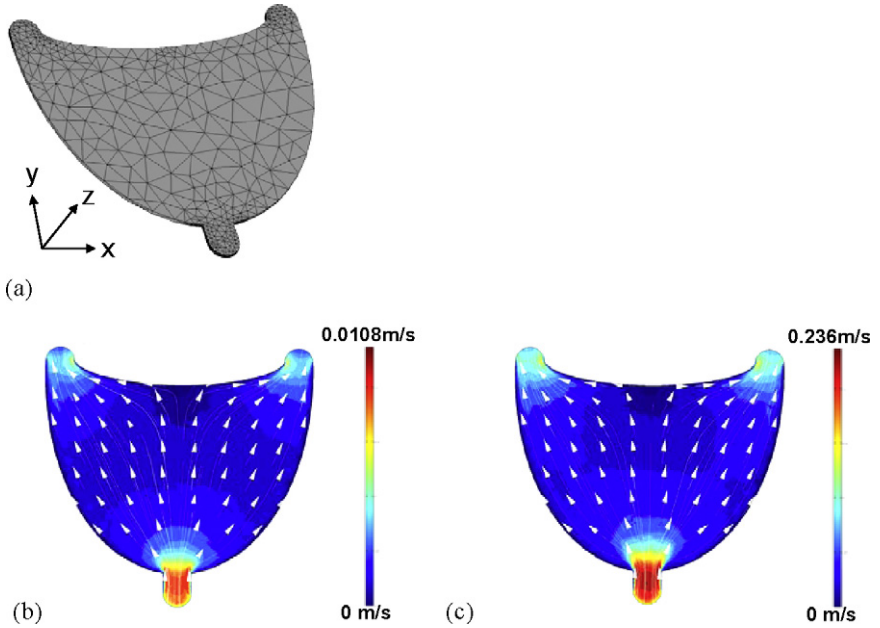

Fig. 2. 3D finite element analysis of flow in the device. (a) Simulation mesh of 5483 elements, (b) simulated velocity field (4 ml min^{-1}, 400 μm thickness), and (c) simulated velocity field (10 ml min^{-1}, 400 μm thickness).

absence of electrolyte membrane, which reduces the cost of the electrolyzer.

100 mm (4 in.) diameter silicon wafers were used to make our devices. In order to get four devices from each wafer, we limit the size of each device to an area of 36 mm × 36 mm. The reaction chamber is chosen to have one inlet for the electrolyte and two outlets, one for the hydrogen with excess electrolyte and one for oxygen with excess electrolyte. The shape of the chamber is designed such that the electrolyte flow is directed into two streams under a large range of inlet flow rates. In general, the flow pattern inside the chamber is a nonlinear function of the flow rate. We utilize FEMLAB to perform three-dimensional finite element analysis of the flow inside the reaction chamber. As shown in Fig. 2(a), a total of 5411 elements are used for the grid of the 3D electrolyzer flow chamber which has a thickness of 400 μm. The volume of the chamber is approximately 200 mm^3. The properties of working fluid, 28 wt% KOH solution, are approximated using water properties. Flow is forced into the chamber at the inlet at a given flow rate, and exits from both outlets with a boundary condition of ambient pressure. A no-slip boundary condition is applied at chamber walls. In a flow rate range of 1–10 ml min^{-1}, corresponding to an entrance velocity range of 0.0108–0.236 m s^{-1}, the flow is laminar. The fluid flows through the chamber following two paths of streams, as shown in Fig. 2(b) and (c). The fluid crossing the anode surface heads towards the "anode exit" while that crossing the cathode surface heads towards the "cathode exit" without interaction. Assuming that the gas bubbles generated from anode and cathode are carried by the fluid flow, oxygen and hydrogen could be collected separately from their designated exits. Vortex flow is expected at higher flow rates, which would cause undesired mixing of the two gases within the chamber.

The two electrodes inside the chamber are designed and placed at the regions where there is a distinct flow stream directed to an outlet. Hydrogen bubble generated at the cathode is carried to one output by one flow stream and oxygen bubble generated at the anode is carried to the second output by another flow stream. The process of gas generation at the cathode can be described as follows [18]. Similar process occurs at the anode. External current provides the energy for electrochemical reaction to form molecular hydrogen which dissolves in the electrolyte. Small bubbles are nucleated and formed from supersaturation sites on or near the electrode. Images of the entire device and 10–50 μm bubbles on top of an electrode are shown in Fig. 3. Growth of bubble is achieved by diffusion of dissolved gas. The bubble is maintained on the electrode by a combination of forces such as buoyancy, superficial tension, flow pressure, inertia and electrostatic forces. When the force on the bubble becomes greater than the adhesion force on the electrode, the bubble is detached from the electrode and moved with the flow stream to the outlet. It is well known that the growth and detachment of the bubble lead to potential increase and jump in the voltage response. In fact, the bubble average radius and mean detachment rate can be calculated from the noise properties of the fluctuating voltage potential [19]. In a typical electrolyzer, the gas bubble is extracted by buoyancy. In our planar electrolyzer, the gas bubble is extracted primarily by laminar flow. In general, the bubble generation efficiency and rate can be increased by increasing the available surface area of the electrode and by increasing the flow rate of the electrolyte. Bubbles should be extracted rapidly so that nucleation site becomes available for more hydrogen generation.

3. Fabrication

Platinum was utilized as the electrode material because it is an excellent catalyst with a large rate of production per unit area [20], is mechanically and chemically stable and is suitable for large area coating. The platinum is deposited as thin film on a silicon oxide on silicon substrate to reduce catalyst loading, i.e. mass of precious metal. One important issue is adhesion to the oxide surface, because platinum, by itself, does not stick to oxide and can be easily delaminated. One solution is an adhesion layer. Both titanium and chromium metal have been used as an intermediate sticking layer to attach platinum to silicon oxide. We look at the Pourbaix diagrams for titanium and chromium which describes the tendency of a metal electrode to corrode in the presence of a solution of a given pH. Titanium was chosen for our final device because it is a more stable material than chromium in a high pH electrolyte. In our experiments, we have fabricated devices using both chromium and titanium. Although we have not performed extensively long-term studies on the corrosion of the electrode, we find titanium to be more durable as long as it is covered by platinum and is not extensively exposed to the electrolyte.

A schematic of the fabrication steps is shown in Fig. 4. The device is made of two layers: the electrode layer and the fluidic chamber layer. Polydimethylsiloxane (PDMS) has the advantage of low cost, high flexibility, inertness and optical transparency. The bonding of PDMS on silicon has been shown to withstand a pressure of 435 kPa [21]. Although PDMS is semi-permeable to hydrogen, with a measured permeability coefficient of 950 Barrer [22], it is water proof and sturdy enough for our prototype development of the planar electrolyzer.

The electrode layer is patterned on silicon oxide wafer using positive photoresist (Shipley) and standard photolithography techniques. Silicon oxide layer is used to electrically isolate the electrodes from the silicon substrate. In a two-step process, 20 nm of titanium metal are deposited, followed by 200 nm of platinum by electron-beam evaporation under 10^{-6} Torr vacuum. The final electrodes are obtained after a lift-off in acetone.

The fabrication of the PDMS fluidic chamber starts with construction of a mold using SU-8 2100, an epoxy-based negative photoresist, on a silicon wafer. SU-8 2100 (MicroChem Corp.) is

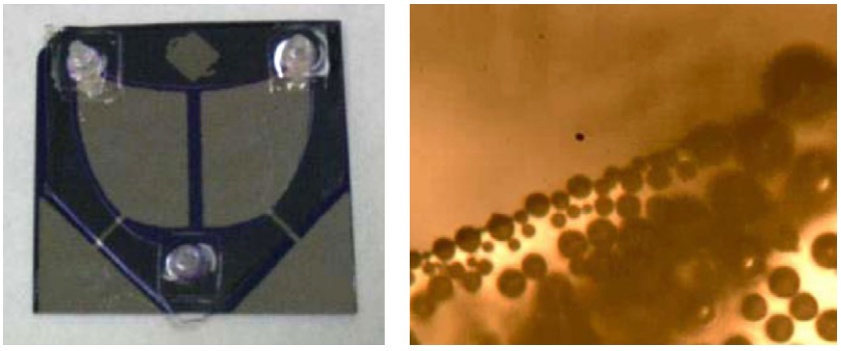

Fig. 3. Photo of a planar electrolyzer and a microscope image of bubbles generated on top of a Pt electrode. Note that there is no bubble formed on top of bared oxide.

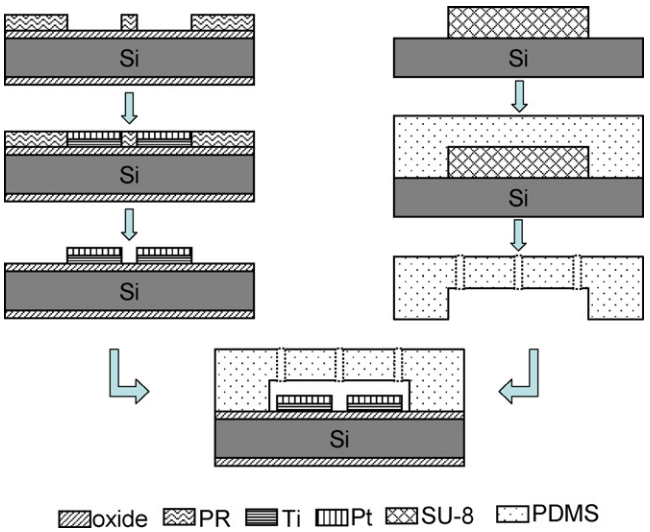

Fig. 4. Process flow for fabrication of the planar electrolyzer.

spin-coated on the wafer using a two-layer technique to form a thickness of 400 μm. The SU-8 is patterned and developed to realize the chamber structure. The process is complete after a hard bake process at 100 °C for 20 min, and a treatment of Omnicoat (MicroChem Corp.) for easy release of the replicas.

PDMS base and curing agent (Dow Corning) are mixed at a ratio of 10:1. The mixture is poured onto the mold and cured for more than 48 h at room temperature. PDMS fluid chamber layer is obtained after peeling the PDMS replica from the mold, and puncturing fluid inlet/outlet holes. Both the fluid chamber surface and the electrode surface are treated using O_2 plasma, and are immediately brought into contact with alignment to form the bonding of the two layers. Finally, the adapters are bonded at the inlet and outlets of the fluidic chamber for connection with the external fluid handling system using tubing. The nominal thickness of the wafer is 525 μm and the total thickness of the device is approximately 3 mm. The volume of the chamber is estimated to be about 200 mm^3.

4. Experiment

The experimental setup is shown in Fig. 5. A syringe pump (Harvard PHD-2000) is used to drive the KOH solution at a constant flow rate into the chamber. At room temperature, the greatest KOH/H_2O conductivity is achieved at 28 wt%, with a conductivity of 0.6 S cm^{-1} [23]. A power supply is connected to the anode and cathode providing input voltage to the electrolyzer, while a multimeter measures the current output.

To investigate the effect of KOH solution flow rate on output current, an input voltage of 3 V is applied across the electrodes while the output current is collected at various flow rates. The effect of flow rate on output current is shown in Fig. 6. A linear increase of current with higher flow rates for a fixed voltage was observed. This is attributed to increased bubble generation caused by increased efficiency of bubble removal. The hydrogen generation is estimated from the measured current and is shown on a separate axis. We make the approximation that all the current above the hydrogen generation threshold goes into the generation of hydrogen. In our experiment, we find that the amount of gas generated per cell is small such that we are unable to accurately obtain the gas flow rate using a flow meter.

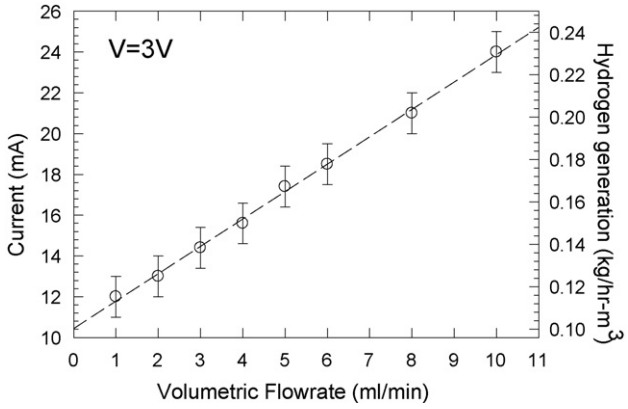

Fig. 6. Effect of flow rate on current for a voltage of 3 V. Dashed line is a least square linear fit to data. Separate axis shows the hydrogen generation. In calculation of the volume, we use the device dimensions of 36 mm × 36 mm × 3 mm. Error bars show the fluctuation in the measured current during the experiment.

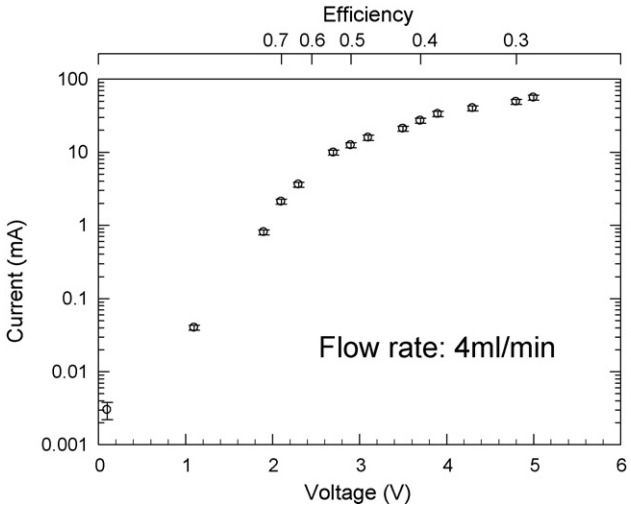

Fig. 7. Tafel plot of log current as a function of voltage for a flow rate of 4 ml min^{-1}. Error bars show the fluctuation in the measured current during the experiment. Efficiency is shown on separate axis.

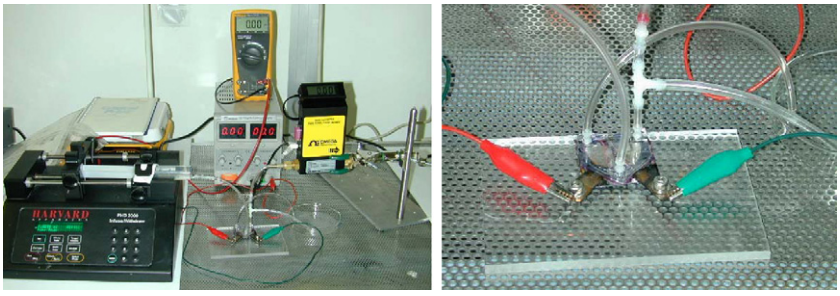

Fig. 5. Experimental setup.

The relationship of current- voltage characteristic of our device is measured at a fixed electrolyte flow rate. The results, shown in Fig. 7, demonstrate a linear relationship in the range of 3–5 V above the hydrogen generation threshold. The hydrogen generation threshold is estimated to be about 1.9 V. We observe that under steady conditions, constant temperature and flow rate, there is a small fluctuation of the observed current. The variation of the current is shown as error bar in the plot. The high overpotential is attributed to parasitic resistance of the device and to interfacial phenomenon [24].

5. Discussion

The operating voltage, V_{cell}, to drive an electrolysis cell at a current I at standard condition for a closed cell is

$$V_{cell} = \frac{-\Delta A^0}{nF} + IR + \sum \eta \quad (1)$$

where $\Delta A^0 = 233.1\ \text{kJ mole}^{-1}$, n is number of electron transferred, F is Faraday's constant, R is Ohmic resistance of cell and $\sum \eta$ represents the sum of the cathode, anode and concentration overpotentials [25]. Unlike an open cell, where the pressure and temperature are assumed to be constant, for a closed cell such as our planar reactor, we have the volume and temperature to be constant. The electrolyzer efficiency is related to the operating voltage by

$$\eta_{EL} = \frac{1.47}{V_{cell}} \frac{i - i_{loss}}{i} \frac{\eta_{DC}}{1+\xi} \quad (2)$$

where i is the operating current density (A cm^{-2}), i_{loss} is the internal current and hydrogen loss (A cm^{-2}), η_{DC} is the efficiency of DC/AC voltage regulator and ξ is the ratio between parasitic power and net power applied to the electrolyzer [14]. The efficiency is inversely proportional to the cell voltage, which is determined by the current density and the hydrogen production per unit electrode area. In general, higher voltage leads to higher hydrogen production but lower efficiency. The peak hydrogen production is typically limited by the corrosion voltage of the electrodes.

We can calculate the efficiency of our device by using (2). Assuming the internal current, hydrogen collection and permeation loss are low, so that $i_{loss} \ll i$, $\eta_{DC} \approx 1$ and $\xi \approx 1$, we calculate the efficiency as a function of hydrogen generation for our device. This is shown in a separate axis in Fig. 7. We can see that for our planar device (Fig. 6), we achieve a hydrogen generation density of $0.23\ \text{kg h}^{-1}\ \text{m}^{-3}$ and an efficiency of 48% with a flow rate of $10\ \text{ml min}^{-1}$ and cell voltage of 3 V. Higher efficiency is attained at lower voltages.

Higher efficiency can also be achieved by lowering the overpotentials. This reduction can be accomplished by using a different type of electrode such as nanostructured catalysis [26] and different electrolyte. For example, by utilizing Pt black and H_2SO_4 32 wt% electrolyte, we have reduced the threshold voltage for hydrogen generation to about 1.6 V [27,28]. However, we also find that the strong acidic electrolyte is incompatible with the PDMS, rendering the PDMS yellowish after immediate exposure.

In conclusion, we have demonstrated a planar electrolyzer with relatively low catalysis loading and small volume. Our device requires a continuous pumping of electrolyte and separates the generated hydrogen and oxygen to different outlets. Although we have emphasized mainly on hydrogen generation, our device can also be applied to oxygen generation, for example in space flight applications. The planar geometry facilitates stacking of multiple reactors in a high-density compact form and integration with planar photovoltaic cells. The planar electrolyzer can be powered directly by photovoltaic cell. A direct PV cell to electrolyzer connection is inherently efficient since it does not require conversion to AC power to connect to the grid and then back to DC to power the electrolyzer. Each conversion step results in approximately 3–5% loss, leading to a saving of 6–10% in efficiency. A local distributed hydrogen generator bypasses the problem of long distance hydrogen transport and provides a fuel source direct to small-scale applications.

Acknowledgements

The authors at The University of Arizona acknowledge funding support from the Arizona Research Institute for Solar Energy. The devices are fabricated at the Nano/Micro Fabrication Center, The University of Arizona, with the Pt deposition done at the University of Minnesota Nanofabrication Center.

References

[1] J. Ohi, J. Mater. Res. 20 (2005) 3180–3187.
[2] M.M. Halmann, M. Steinberg, Greenhouse Gas Carbon dioxide Mitigation: Science and Technology, CRC Press, 1999, pp. 1–13.
[3] J.R. Bolton, Solar Energy 57 (1996) 37–50.
[4] S. Licht, J. Phys. Chem. B 107 (2003) 4253–4260.
[5] A. Kogan, Int. J. Hydrogen Energy 25 (2000) 739–745.
[6] J. Funk, Int. J. Hydrogen Energy 26 (2001) 185–190.
[7] J. Miyake, W.T. Schnackenberg, J. Arai, T. Asada, J. Biosci. Bioeng. 88 (1999) 659–663.
[8] E. Amouyal, Solar Energy Mater. 38 (1995) 249–276.
[9] M. Gratzel, Nature 414 (2001) 338–344.
[10] B. Esper, A. Badura, M. Rogner, Trends Plant Sci. 11 (2006) 543–549.
[11] S. Khan, M. Al-Shahry, W. Ingler Jr., Science 297 (2002) 2243–2245.
[12] M. Ni, M.K.H. Leung, D.Y.C. Leung, Chem. Eng. Technol. 29 (2006) 636–642.
[13] R. Kothari, D. Buddhi, R.L. Sawhney, Int. J. Hydrogen Energy 30 (2005) 261–263.
[14] F. Barbir, Solar Energy 78 (2005) 661–669.
[15] S. Licht, G. Hodes, R. Tenne, J. Manassen, Nature 326 (1987) 863–864.
[16] P.A. Lehman, C.E. Chamberlin, G. Pauletto, M.A. Rocheleau, Int. J. Hydrogen Energy 22 (1997) 465–470.
[17] Y. Yamada, N. Matsuki, T. Ohmori, H. Mametsuka, M. Kondo, A. Matsuda, E. Suzuki, Int. J. Hydrogen Energy 28 (2003) 1167–1169.
[18] C. Gabrielli, F. Huet, M. Keddam, J. Appl. Electrochem. 15 (1985) 503–508.
[19] C. Gabrielli, F. Huet, M. Keddam, A. Sahar, J. Appl. Electrochem. 19 (1989) 683–696.
[20] J.O'M. Bockris, A.K.N. Reddy, M. Gamboa-Aldeco, Modern Electrochemistry 2A, 2nd ed., Kluwer Academic, 2000, p. 1285.
[21] S. Li, S. Chen, IEEE Trans. Adv. Packaging 26 (2003) 242–247.
[22] T.C. Merkel, R.P. Gupta, B.S. Turk, B.D. Freeman, J. Membrane Sci. 191 (2001) 85–94.
[23] R. Gilliam, J. Graydon, D. Kirk, S. Thorpe, Int. J. Hydrogen Energy 32 (2007) 359–364.
[24] H. Matsushima, T. Nishida, Y. Konishi, Y. Fukunaka, Y. Ito, K. Kuribayashi, Electrochim. Acta 48 (2003) 4119–4125.
[25] C. Neagu, H. Jansen, H. Gardeniers, M. Elwenspoek, Mechatronics 10 (2000) 571–581.
[26] S. Kim, N. Koratkar, T. Karabacak, T.M. Lu, Appl. Phys. Lett. 88 (2006) 263106.
[27] Metrohm Corp., Platinization of platinum electrodes and conductivity measuring cells, Application Bulletin No. 64/2e.
[28] B. Yazici, Turk. J. Chem. 23 (1999) 301–308.